Hepatocyte-specific deletion of adipose triglyceride lipase (adipose triglyceride lipase/patatin-like phospholipase domain containing 2) ameliorates dietary induced steatohepatitis in mice

Fuchs, Claudia D; Radun, Richard; Dixon, Emmanuel D; Mlitz, Veronika; Timelthaler, Gerald; Halilbasic, Emina; Herac, Merima; Jonker, Johan W; Ronda, Onne A H O; Tardelli, Matteo

Published in:
Hepatology

DOI:
10.1002/hep.32112
10.1002/hep.32112

Document Version
Final author's version (accepted by publisher, after peer review)

Publication date:
2022

Article type : Original

Hepatocyte-specific deletion of adipose triglyceride lipase (ATGL/PNPLA2) ameliorates dietary induced steatohepatitis in mice

Claudia D Fuchs[1], Richard Radun[1], Emmanuel D Dixon[1], Veronika Mlitz[1], Gerald Timelthaler[2], Emina Halilbasic[1], Merima Herac[3], Johan W Jonker[4], Onne A H O Ronda[5], Matteo Tardelli[1,6], Guenter Haemmerle[7], Robert Zimmermann[7], Hubert Scharnagl[8], Tatjana Stojakovic[9], Henkjan J Verkade[5] and Michael Trauner[1*]

[1]Hans Popper Laboratory of Molecular Hepatology, Division of Gastroenterology and Hepatology, Department of Internal Medicine III, Medical University of Vienna, Austria

[2]Institute for Cancer Research, Internal Medicine I, Medical University of Vienna, Vienna, Austria

[3]Clinical Institute of Pathology, Medical University Vienna, Vienna, Austria

[4]Department of Pediatrics, Section of Molecular Metabolism and Nutrition, University of Groningen, University Medical Center Groningen, The Netherlands.

[5]Pediatric Gastroenterology and Hepatology, University of Groningen, University Medical Center Groningen, The Netherlands

[6]Division of Gastroenterology and Hepatology, Department of Medicine, Weill Cornell Medical College, New York, United States of America

[7]BioTechMed-Graz, Graz, Austria; Institute of Molecular Biosciences, University of Graz, Graz, Austria

[8]Clinical Institute of Medical and Chemical Laboratory Diagnostics, Medical University of Graz, Austria

[9]Clinical Institute of Medical and Chemical Laboratory Diagnostics, University Hospital Graz, Austria

This article has been accepted for publication and undergone full peer review but has not been through the copyediting, typesetting, pagination and proofreading process, which may lead to differences between this version and the Version of Record. Please cite this article as doi: 10.1002/HEP.32112

*** Corresponding author:**

Michael Trauner, MD

Professor and Chair of Gastroenterology and Hepatology

Division of Gastroenterology and Hepatology, Department of Internal Medicine III,

Medical University of Vienna, Waehringer Guertel 18-20, A-1090 Vienna, Austria.

Tel: +43 1 40 40047410

Email: michael.trauner@meduniwien.ac.at

Keywords: NAFLD/NASH, lipolysis, PPARα, PPARδ

Electronic word count: 4469

Number of figures: 8 main figures, 11 supporting figures, 2 supporting tables

Conflict of interest statement: Michael Trauner has served as speaker for Falk Foundation, Gilead, Intercept and MSD; he has advised for Albireo, BiomX, Boehringer Ingelheim, Falk Pharma GmbH, Genfit, Gilead, Intercept, Jannsen, MSD, Novartis, Phenex, Regulus and Shire. He further received travel grants from Abbvie, Falk, Gilead and Intercept and research grants from Albireo, Alnylam, Cymabay, Falk, Gilead, Intercept, MSD Takeda and UltraGenyx. He is also co-inventor of patents on the medical use of NorUDCA filed by the Medical Universities of Graz and Vienna.All other authors have no financial disclosures concerning this study to report.

Authors' contributions: CDF: Conceptualization, Data curation, Writing – original draft, Writing – review & editing; RR: Data curation; EDD: Data curation; VM: Data curation; GT: Data curation; EH: Data Curation;

MH: Data curation; JWH: Data curation; OR: Data curation; Matteo Tardelli: Data curation; GH: Writing – review & editing; RZ: Writing – review & editing; HS: Data curation, Writing – review & editing; TS: Writing – review & editing; HJV: Writing – review & editing; Michael Trauner: Conceptualization, Funding acquisition, Writing – review & editing

Financial support: This work was supported by the grant F7310-B21 from the Austrian Science Foundation (to Michael Trauner).

Acknowledgements: The authors thank Nicole Auer, Victoria Kunczer both from the Hans Popper Laboratory of Molecular Hepatology, Division of Gastroenterology and Hepatology, Department of Internal Medicine III, Medical University of Vienna, Austria as well as Roos Eilers from the Pediatric Gastroenterology and Hepatology, University Medical Centre Groningen, University of Groningen, The Netherlands, for their excellent technical support.

Abstract

Background and Aims: Increased FA flux from adipose tissue to the liver contributes to the development of NAFLD. Since free FAs are key lipotoxic triggers accelerating disease progression, inhibiting ATGL/PNPLA2, the main enzyme driving lipolysis, may attenuate steatohepatitis.

Approach and results: Hepatocyte-specific ATGL knockout (ATGL LKO) mice were challenged with MCD or HFHC diet. Serum biochemistry, hepatic lipid content and liver histology were assessed. Mechanistically, hepatic gene and protein expression of lipid metabolism, inflammation, fibrosis, apoptosis and ER stress markers were investigated. DNA binding activity for PPARα and PPARδ was measured. After sh-RNA mediated ATGL-knockdown, HepG2 cells were treated with LPS or OP21 to explore the direct role of ATGL in inflammation *in vitro*. Upon MCD and HFHC challenge, ATGL LKO mice showed reduced PPARα and increased PPARδ DNA binding activity when compared to challenged WT mice. Despite histologically and biochemically pronounced hepatic steatosis, dietary challenged ATGL LKO mice showed lower hepatic inflammation, reflected by reduced number of MAC-2 and MPO positive cells and low mRNA expression levels of inflammatory markers (such as IL1β and F4/80) when compared to WT mice. In line, protein levels of ER stress markers PERK and IRE1α were reduced in ATGL LKO MCD fed mice. Accordingly, pretreatment of LPS treated HepG2 cells with the PPARδ agonist GW0742, suppressed mRNA expression of inflammatory markers. Additionally, ATGL-knockdown in HepG2 cells attenuated LPS/OP21-induced expression of pro-inflammatory cytokines and chemokines such as Cxcl5, Ccl2 and Ccl5.

Conclusions: Low hepatic lipolysis and increased PPARδ activity in ATGL/PNPLA2 deficiency may counteract hepatic inflammation and ER stress despite increased steatosis. Therefore, lowering hepatocyte lipolysis via ATGL inhibition represents a promising therapeutic strategy for the treatment of steatohepatitis.

Abbreviations

ALT	alanine amino transferase
AP	alkaline phosphatase
AST	aspartate amino transferase
ATGL	adipose triglyceride lipase
DBA	DNA binding activity
FA	fatty acid
ER	endoplasmic reticulum
HFHC	high fat high carbohydrate
IHC	immunohistochemistry
IRE1α	inositol-requiring enzyme 1 α
KO	knockout
LPS	lipopolysaccharide (endotoxin)
LW	liver weight
MCD	methionine-choline-deficient
MPO	myeloperoxidase
NAFLD	nonalcoholic fatty liver disease
NEFA	non-esterified fatty acid
NASH	nonalcoholic steatohepatitis
PERK	protein kinase R-like endoplasmic reticulum kinase
PDK4	pyruvate dehydrogenase lipoamide kinase isozyme 4
PPARα	peroxisome proliferator-activated receptor α
PPARδ	peroxisome proliferator-activated receptor δ
SD	standard deviation
TG	triglyceride

WT	wild-type

Introduction

As a consequence of the pandemic of obesity and diabetes, non-alcoholic fatty liver disease (NAFLD) has become a leading cause of liver disease in the Western world [1, 2]. As such, more than 20% of the general population [3] and 75% of obese individuals [4] develop NAFLD. NAFLD is characterized by benign hepatic fat accumulation (i.e., steatosis) which can progress to non-alcoholic steatohepatitis (NASH), advanced fibrosis, cirrhosis, and cancer [5, 6], with inflammation as central feature in the disease progression from benign steatosis to the more severe stages of the disease spectrum [7]. Increased free fatty acids (FAs) are key lipotoxic triggers driving hepatocyte injury and inflammation and the progression from NAFLD to NASH [8]. Increased FA flux from adipose tissue to the liver due to insulin resistance as well as their release from hepatocellular TG stores may critically determine hepatic FA concentrations and thereby lipotoxicity [9].

However, FAs have also other powerful roles and are directly involved in cellular signaling pathways and regulation of gene transcription [10]. Specifically, FAs are known to activate potential anti-inflammatory PPAR signaling [11]. Adipose triglyceride lipase (ATGL) as the major enzyme in TG breakdown may provide ligands for FA-regulated transcription factors, such as PPARα and δ [12-16], thereby modulating hepatic inflammation and disease progression. ATGL-catalyzed TG hydrolysis is a prerequisite for functional PPARα signaling, suggesting that FAs deriving from TG stores activate PPARα and consequently the expression of genes for mitochondrial FA oxidation [13]. This aspect is discussed controversially for PPARδ [16, 17]. Despite the difference in their way of activation, both PPARα and PPARδ seem to have a crucial role in the protection against NAFLD/NASH development [18]. Accordingly, PPARα KO mice fed a methionine choline deficient (MCD) diet develop more severe steatohepatitis than WT mice [19, 20] while treatment of hApoE2 KI/ PPARα KO mice with a PPARα/δ dual agonist significantly improved MCD diet induced liver injury [21]. Interestingly, PPARδ can compensate for the absence of PPARα in regulating FA homeostasis in skeletal muscle [22]. To test whether this appealing concept is also relevant in liver, this study was designed to investigate whether PPARδ signaling may compensate for impaired PPARα

signaling in the liver, thereby attenuating hepatic inflammation and subsequent progression from steatosis to steatohepatitis. For this purpose, hepatocyte-specific ATGL KO mice (with impaired PPARα signaling) were subjected to MCD diet, a well-established model of steatohepatitis. Despite several disadvantages of MCD diet such as absence of obesity and insulin resistance, it is a suitable model to initiate profound lipolysis in adipose tissue resulting in increased FA flux from the periphery to the liver [23]. Additionally, and to also obtain insights into the metabolic state of the disease hepatocyte-specific ATGL KO mice were fed a high fat high carbohydrate rich diet. Using this experimental approach, we observed that absence of ATGL/PNPLA2 in hepatocytes results in steatosis but reduced inflammation most likely via activation of hepatic PPARδ signaling as an adaptation to loss of PPARα signaling.

Materials and Methods

Animals experiments: C57/BL6 ATGL f/f were crossed with C57/BL6 Alb-Cre mice to generate hepatocyte-specific ATGL KO mice. ATGL f/f mice were used as control animals. ATGL f/f were kindly provided by Erin E Kershaw [24]; (JAX stock number of ATGL f/f mice: 024278). Male 8 week old animals were fed a methionine choline deficient (MCD) diet (obtained from SAFE - Scientific Animal Food & Engineering) for 5 weeks *ad libitum*. Female 5 week old animals were fed a high fat diet plus fructose/sucrose in drinking water (HFHC) for 17 weeks (high fat diet: D12331, *Research Diets*, New Brunswick, NJ), plus 42g/L fructose/sucrose in drinking water; control diet: D12328, *Research Diets*, New Brunswick, NJ). These animal studies were approved by the Animal Ethics Committee of the Medical University of Vienna and the Federal Ministry of Science, Research and Economy (BMWFW-66.009/0117-II/3b/2013) and was performed according to the Animal Research: Reporting of *In Vivo* Experiments (ARRIVE) guidelines.

Human liver sections: Human liver paraffin sections of NAFLD patients with different stages of fibrosis (F0-F4) were kindly provided by the Department of Pathology, Medical University of Vienna. Patients gave informed consent at the time of recruitment and their records were anonymized and de-identified. Patient's data and pathologic evaluations were approved by Ethics Committee of the Medical University of Vienna (EC: 747/2011). Detailed clinical data of the patient cohort are provided in Ref. [25].

Liver Histology: Liver tissue was fixed in 4% neutral buffered formaldehyde solution for 24 hours, embedded in paraffin, and stained with hematoxylin and eosin (H&E) or Sirius Red. To quantify and characterize the hepatic inflammatory cell infiltrate immunohistochemistry for MAC-2$^+$ cells and immunofluorescence of myeloperoxidase (MPO)$^+$ cells was performed. Oil red o (ORO) staining was performed on 7µM thick cryosections as described previously [26]. To obtain the degree of steatosis and inflammation computational quantification was done with Image J 1.51j8. The NAFLD grading shown in Supporting table 1 and 2 is based on computational analysis of H&E (macrovesicular & microvesicular steatosis) and MAC-2$^+$ (inflammatory cells) sections. The scoring is in accordance to Ref. [27].

Serum Analysis:
At the end of experiment blood was collected from the vena cava and centrifuged for 15 min at 4500 rpm. Serum was stored at -80°C until analysis.

DNA binding activity of PPARα and PPARδ: PPARα as well as PPARδ activity was assayed using an enzyme-linked immunosorbent assay-based PPARα Transcription Factor Assay Kit (Abcam) according to the manufacturer's instructions. Nuclear proteins were isolated from liver using NE-PER nuclear and cytoplasmic extraction kit (Abcam) according to the manufacturer's instructions. Binding activity was measured at 450 nm (minus the blank) and calculated as relative activity to the control.

Western blotting: Protein isolation and western blotting was performed as described previously [28].

RNA isolation and qRT-PCR analysis: Tissues were snap frozen in prechilled 2-methylbutane and stored in liquid nitrogen. RNA was extracted using TRIzol reagent (Invitrogen, Carlsbad, CA) according to manufacturer's instructions. 1.5µg of RNA was used for complementary DNA synthesis using random hexamer primer (Applied Biosystems) and Superscript II reverse transcriptase (Invitrogen, Carlsbad, CA) according to manufacturer's instructions. 1:20 dilution of the cDNA was used for qRT-PCR using SYBR Green Master Mix (Applied Biosystems) and was performed using AB7900 Real-Time PCR system (Applied Biosystems). Reactions were performed in duplicates and relative mRNA levels were quantified using a calibration dilution curve normalized to the housekeeping genes. mRNA levels were normalized to 36b4 as housekeeping gene which did not vary between groups.

Liver TGs, NEFA and fatty acyl chain profiling: Hepatic lipids were extracted and analyzed by gas chromatography as described previously [29].

Cell culture: HepG2 and Hepa1c1c7 cells (American Type Culture Collection, Manassas, VA) were grown in Dulbecco`s modified Eagle`s medium and knocked down for ATGL (ATGL KD) using a lentivirus containing a short hairpin RNA against ATGL as described previously [26]. WT and ATGL KD cells were treated with LPS for 6h or oleic

acid (OA): palmitic acid (PA) in a ratio 2:1 (OP21). OA concentration: 1,2mM; PA concentration: 0,6mM. Furthermore, in a separate experiment HepG2 WT cells were pretreated for 18h with the PPARδ agonist GW0742 prior to 6h LPS treatment. THP1 and RAW 264.7 cells (American Type Culture Collection, Manassas, VA) were grown in Dulbecco`s modified Eagle`s medium and incubated for 6h with medium taken from WT and ATGL KD cells with and without LPS or incubated 24h with medium taken from WT and ATGL KD cells with and without OP21 treatment.

Cytokine analysis: Proteome profiler mouse XL cytokine array from R&D Systems was assessed according to manufacturer's instructions.

Statistical analysis: Results were evaluated using SPSS V.27.0. Statistical analysis was performed using student´s unpaired 2-tailed t test. In the MCD setting data are reported as means of WT Ctrl n=5; ATGL LKO Ctrl n=7; WT MCD n=7; ATGL LKO MCD n=9 animals per group +/-SD. In the HFHC setting data are reported as means of WT Ctrl n=7; ATGL LKO Ctrl n=5; WT HFHC n=7; ATGL LKO HFHC n=5 animals per group +/-SD. A p value ≤0.05 was considered as statistically significant.

Results

Absence of hepatic ATGL reduces PPARα activity in MCD-induced steatohepatitis.

Previous studies have demonstrated that global ATGL KO mice challenged with methionine choline deficient (MCD) diet develop more severe steatohepatitis because of impaired PPARα signalling due to lack of free FAs serving as PPARα ligands [28]. To investigate the specific role of hepatic ATGL in development of steatohepatitis, hepatocyte-specific ATGL KO (ATGL LKO) and floxed control mice (WT) were fed a MCD diet for 5 weeks. In accordance with the findings in global ATGL deficiency, also ATGL LKO mice showed reduced PPARα DNA binding activity (Supporting Figure 1A) when compared to MCD fed WT mice. Accordingly, mRNA expression levels of established PPARα target genes were significantly lower in MCD fed ATGL LKO compared to MCD fed WT animals (Supporting Figure 1B).

MCD feeding aggravates development of hepatic steatosis.

Since impaired PPARα signalling and consequently defective FA oxidation potentially contributes to development of steatosis, next hepatic TG content was assessed. In line with the observations at the histological level, quantification of hepatic TG significantly increased TG levels in ATGL LKO mice already at chow diet, and levels were further boosted by the MCD challenge (Figure 1A and B, Supporting table 1). This observation was confirmed by oil red O staining (Figure 1C). Serum levels of liver transaminases ALT and AST were elevated on MCD independent of the genotype while alkaline phosphatase (AP) was solely increased in ATGL LKO mice upon the dietary challenge (Figure 1D). Serum levels of total cholesterol, TG as well as NEFA were reduced upon MCD feeding in both, WT and ATGL LKO mice (Figure 1D).

Absence of hepatic ATGL ameliorates hepatic inflammation in MCD diet-induced steatohepatitis.

Besides steatosis, inflammation is a major hallmark of hepatic steatohepatitis. Therefore, we investigated inflammatory parameters such as MAC-2, MPO, *IL1β*, *F4/80* and *TNFα* in mice kept on MCD. Surprisingly, immunohistochemistry (IHC) revealed less MAC-2 and MPO positive cells in livers of ATGL LKO than in WT mice under MCD challenge

(Figure 2A and B). Accordingly, mRNA levels of inflammatory markers were significantly decreased in ATGL LKO animals under MCD condition in comparison to challenged WT animals (Supporting Figure 2A). Of particular interest, sirius red and Collagen 1 staining (as a marker for fibrosis) were similar in ATGL LKO compared to WT mice indicating no differences in collagen deposition. However, mRNA levels of *Col1a1*, *Col1a2 and Tgfβ* were increased in both, WT and ATGL LKO MCD fed mice (Supporting Figure 3).

Hepatic ATGL deficiency mitigates ER stress in MCD diet-induced steatohepatitis.

Since hepatic inflammation may trigger hepatic endoplasmic reticulum (ER) stress, we assessed protein and mRNA levels of ER stress relevant genes. The ER stress sensors PERK and IRE1α showed markedly lower protein expression levels in ATGL LKO mice compared to WT mice upon MCD feeding (Figure 2C). In line, mRNA expression of *ErDj4* and *Grp78* followed the same pattern (Supporting Figure 2B). Of note, mRNA levels of the apoptotic markers *Chop* and *Bad* as well as protein levels of cleaved caspase 3 were increased upon MCD feeding independent of the genotype (Supporting Figure 2C and D).

Absence of hepatic ATGL induces PPARδ binding activity in MCD diet-induced steatohepatitis.

It has been shown previously that PPARδ (but not PPARα) can be activated via FAs directly coming from the serum (not being hydrolysed from endogenous TG stores) [16]. Moreover, PPARδ was also identified to have anti-inflammatory effects under NAFLD conditions [18, 30]. Therefore, we considered augmented PPARδ activation as a possible compensatory mechanism of compromised (anti-inflammatory) PPARα signalling (Supporting Figure 1) and thus a mechanistic explanation for attenuated hepatic inflammation in MCD challenged ATGL LKO mice. DNA binding activity assay revealed increased PPARδ binding activity solely in ATGL LKO MCD fed mice (Figure 3A). Consequently, mRNA expression of PPARδ target *Pdk4* was boosted in ATGL LKO MCD fed animals (Figure 3B). Accordingly, PDK4 protein expression was significantly increased in ATGL LKO MCD fed mice compared to challenged WT mice (Figure 3C). Moreover, intrahepatic FA profiling elucidated enhanced levels of α– and γ–linolenic acid as well as oleic acid, established ligands for PPARδ (Figure 3D). Interestingly, the level of vaccenic acid, which has been shown to maintain PPARδ in its activated conformation

[31, 32], was reduced in WT mice upon MCD feeding while in ATGL LKO mice levels stayed normal (Supporting Figure 4). Of note, intrahepatic concentration of anti-inflammatory palmitoleic acid, which is not related to PPAR signalling [33], was exclusively reduced in WT mice upon MCD diet and accordingly normal in ATGL LKO mice on MCD (Supporting Figure 4).

Absence of hepatic ATGL reduces PPARα activity in HFHC-induced steatohepatitis.

To investigate whether PPARα signalling is disturbed in ATGL-LKO mice in a second metabolic model, PPARα DNA binding activity was assessed under high fat high carbohydrate (HFHC) conditions. Accordingly, ATGL LKO mice showed reduced PPARα DNA binding activity (Supporting Figure 5A) when compared to HFHC fed WT mice. In line, mRNA expression levels of established PPARα target genes were significantly lower in HFHC fed ATGL LKO compared to HFHC fed WT animals (Supporting Figure 5B).

HFHC feeding aggravates development of hepatic steatohepatitis.

In accordance with the observations of increased hepatic lipid load, at the histological level, quantification of hepatic TG revealed a significant increase in ATGL LKO mice already at chow diet, further elevated by HFHC application (Figure 4A and B, Supporting table 2). This finding was confirmed by oil red O staining (Figure 4C). Serum levels of liver transaminases ALT and AST were already elevated in ATGL LKO mice at baseline. While in WT mice HFHC challenge led to a further increase of ALT and AST. In ATGL LKO HFHC fed mice, ALT and AST levels remained unchanged compared to control mice. Alkaline phosphatase (AP) and triglyceride concentration were neither affected by genotype nor by feeding (Figure 4D). Total cholesterol as well as non-esterified fatty acid (NEFA) concentration were increased due to HFHC feeding independent of the genotype (Figure 4D).

Absence of hepatic ATGL ameliorates hepatic inflammation in HFHC diet-induced steatohepatitis.

Investigation of inflammatory parameters such as MAC-2, MPO, *IL1β*, *F4/80* and *Tnfα* revealed that loss of ATGL in the liver attenuated development of hepatic inflammation

induced by HFHC diet. Immunohistochemistry (IHC) conceded less MAC-2 and MPO positive cells in livers of ATGL LKO than in WT mice under HFHC challenge (Figure 5A and B). Accordingly, mRNA levels of inflammatory markers were significantly decreased in ATGL LKO animals under HFHC condition in comparison to challenged WT animals (Supporting Figure 6A). Fibrosis markers such as, Sirius red and Collagen 1 staining were similar in ATGL LKO compared to WT mice indicating no differences in collagen deposition. However, mRNA levels of *Col1a1*, *Col1a2* and *Tgfβ* tended to be decreased in ATGL LKO compared to WT HFHC fed mice (Supporting Figure 7).

Hepatic ATGL deficiency mitigates ER stress in HFHC diet-induced steatohepatitis.

To evaluate whether HFHC feeding induced hepatic ER stress, we assessed protein and mRNA levels of ER stress relevant genes. The ER stress sensors PERK and IRE1α were increased in both, WT and ATGL LKO mice fed with HFHC diet (Figure 5C), while mRNA expression of the downstream target *Grp78* was only significantly increased in WT HFHC fed mice, expression levels of *ErDj4* remained unchanged upon the different groups (Supporting Figure 6B). mRNA levels of the apoptotic marker *Chop* was increased in WT HFHC mice only. mRNA levels of *Bad* as well as protein levels of cleaved caspase 3 were unaffected upon HFHC feeding independent of the genotype (Supporting Figure 6C and D).

Absence of hepatic ATGL induces PPARδ binding activity in HFHC diet-induced steatohepatitis.

DNA binding activity assay revealed increased PPARδ binding activity in ATGL LKO HFHC fed mice (Figure 6A). Accordingly, mRNA expression of PPARδ downstream target *Pdk4* was elevated in ATGL LKO HFHC fed animals (Figure 6B). In line, PDK4 protein expression was significantly increased in ATGL LKO HFHC fed mice compared to control mice (Figure 6C). Intrahepatic FA profiling elucidated unchanged levels of α– and γ–linolenic acid between the groups, while oleic acid levels were already increased in ATGL LKO mice at baseline. HFHC feeding boosted oleic acid concentration in WT but not in ATGL LKO mice (Figure 6D). Concentration of vaccenic acid, known to maintain PPARδ in its activated conformation [31, 32], was increased in ATGL LKO mice already at baseline (Supporting Figure 4B). Of note, intrahepatic concentration of anti-

inflammatory palmitoleic acid, which is not related to PPAR signalling [33], was also induced at baseline in ATGL LKO mice (Supporting Figure 4B).

ATGL knock down protects from LPS and fatty acid induced inflammation *in vitro*.

To investigate whether absence of ATGL in hepatocytes per se may contribute to attenuation of endotoxin induced inflammation (seen in MCD fed animals [34]), ATGL was silenced with shRNA in the human hepatoma cell line HepG2 (Supporting Figure 8A and B). Cells were cultured in a medium without FBS 16h prior to the treatment with LPS as pro-inflammatory stimuli inducing the activation of TLR4 related pathways. After 6h of LPS treatment, mRNA expression of inflammatory markers *Mcp1*, *Cxcl2* and *Tnf*α stayed at basal levels in ATGL knock down (KD) cells while all makers were increased in WT cells (Figure 7A). From another batch of cells, LPS containing medium was removed after 6h and exchanged by empty medium. 24h later the medium was used for protein profiling. Medium taken from WT LPS challenged cells contained the chemokines Osteopontin, IL-8, MIC-1and VEGF. Notably, signals of these proteins were much lower in medium from ATGL KD cells compared to WT cells (Figure 7B). Because chemokines are involved in recruitment and activation of inflammatory cells, cytokine cocktails produced from HepG2 WT and ATGL KD cells after LPS treatment were used to treat the human macrophage cell line THP1 for 6h. THP1 cells treated with medium from HepG2 WT LPS treated cells displayed increased mRNA expression levels of the inflammatory markers *IL1*β, *IL6* and *Mcp1*. In strong contrast, mRNA levels of these genes stayed low in THP1 cells treated with medium from HepG2 ATGL KD LPS treated cells (Figure 7C), arguing for a direct anti-inflammatory effect of reduced ATGL activity in hepatocytes. Of note, to validate the translational effect between human and mouse, the same experiment was performed in a hepatocyte cell line derived from mouse (Hepa1c1c7). Like in the human cell line, loss of ATGL protected murine hepatocytes from LPS induced inflammation (Supporting Figures 8 and 9).

Moreover, to investigate whether loss of ATGL also protects from FA induced inflammation, cells were cultured in medium containing OP21 as pro-inflammatory stimuli. After 24h of OP21 treatment, mRNA expression of inflammatory markers *Mcp1*, *IL1b, IL6* and *Cxcl2* stayed at basal levels in ATGL knock down (KD) cells while all markers were increased in WT cells (Supporting Figure 10A).

Following the same experimental procedure as for the LPS setting, OP21 containing medium was removed after 24h and exchanged by medium without OP21. 24h later the medium consisting secreted cytokines was used for protein profiling. While the medium taken from WT OP21 challenged cells contained the chemokines Osteopontin and IL-8, these signal proteins were not detected in medium from ATGL KD cells (Supporting Figure 10B). The cytokine cocktails produced from HepG2 WT and ATGL KD cells after OP21 treatment were used to treat the human macrophage cell line THP1 for 6h. THP1 cells treated with medium from HepG2 WT OP21 treated cells displayed increased mRNA expression levels of the inflammatory markers *IL1β*, *IL6* and *Mcp1*. In strong contrast, mRNA levels of these genes stayed low in THP1 cells treated with medium from HepG2 ATGL KD OP21 treated cells (Supporting Figure 10C), arguing for a direct anti-inflammatory effect of reduced ATGL activity in hepatocytes.

Activation of PPARδ reduces LPS induced inflammation *in vitro*.

To investigate whether the LPS mediated inflammation seen in HepG2 WT cells, can be counteracted by PPRAδ activation, HepG2 WT cells were pre-treated with the PPARδ agonist GW0742 for 18h prior to 6h LPS incubation (Figure 8). Treatment of WT cells with GW0742 result in increased protein expression of PPARδ downstream target Pdk4 (Figure 8A). The PPARδ anti-inflammatory effect has been linked to inhibition of NFκB signalling, which prompted us to measure protein expression of NFκB subunits. While expression of p50 and p65 subunits were increased in the nuclei of LPS treated HepG2 WT cells, pre-treatment with GW0742 prevented elevated expression levels of both NFκB subunits (Figure 8B). Consequently, expression levels of the pro-inflammatory cytokines *Mcp1, Cxcl2* and *Tnfα* were increased in LPS treated cells whereas expression levels remained low and comparable to control cells upon GW0742 pre-treatment cells (Figure 8C).

PPARδ expression correlates negatively with disease progression.

To clarify whether the murine findings that PPARδ may have a beneficial role in counteracting NAFLD development PPARδ protein expression was investigated in a NAFLD patient cohort consisting patients aged ≥18 years with biopsy-proven NASH [25]. PPARδ expression was found to be reduced in patients with NASH with fibrosis stage 3

(NASH F3) (Supporting Figure 11), arguing for a crucial role of PPARδ in counteracting disease progression.

Discussion

In this study, we investigated the hepatocyte-specific role of ATGL in the development of steatohepatitis by challenging hepatocyte specific ATGL KO (ATGL LKO) mice with MCD as well as HFHC diet. Both diets are common models to induce steatohepatitis leading to endotoxin translocation, steatosis and inflammation. However, despite MCD diet has some limitations, such as absence of obesity and insulin resistance, it reflects several NASH key features such as steatosis and inflammation [35-37]. Importantly, MCD diet induces massive FA flux from adipose tissue to the liver, thus reflecting a key pathogenic step in NASH development since an increased peripheral FA flux has been linked to a 60% increase of hepatic TG content in NAFLD patients [38]. Therefore, the two complementary models used in this study – ATGL LKO mice fed either with MCD or HFHC – offer the opportunity to investigate whether lack of hepatic ATGL (and hence impaired hepatic lipolysis) may increase the susceptibility to hepatic inflammation via altered lipid partitioning and impaired PPARα signalling as demonstrated in global ATGL KO mice [28]. Alternatively, the FA spill-over to the liver could result in activation of compensatory anti-inflammatory mechanism(s) such as increased PPARδ signalling, which was shown to countervail detracted PPARα signalling in skeletal muscle [22].

Our data demonstrate that despite reduced hepatic PPARα signalling, loss of ATGL in the liver attenuates development of hepatic inflammation and ER stress as major events progressing fatty liver disease from simple steatosis to more severe stages of the disease such as steatohepatitis. Although serum markers for liver damage (AST and ALT) were increased at comparable levels in WT and ATGL LKO mice upon dietary challenge, hepatic steatosis was moderately increased in ATGL LKO MCD as well as HFHC fed mice compared to WT MCD and HFHC mice, while inflammatory as well as ER stress markers (in the MCD setting) were significantly reduced. These findings indicate, that counteracting hepatic lipolysis and consequently increasing hepatic TG formation may have a protective role against inflammation and ER stress development.

Interestingly, mRNA expression of fibrosis markers *Col1a1*, *Col1a2* and *Tgfβ* tended to be increased due to MCD as well as HFHC feeding independent of the genotype. However, computational quantification of SR and Collagen 1 IHC did not show

differences between challenged and control animals. This controversy between mRNA and protein expression may indicate that mRNA expression levels do not reflect the polymerization and formation of collagen fibers. Furthermore, these data indicate that to investigate the role of ATGL in development of hepatic fibrosis, the feeding period of 5 weeks MCD and 17 weeks HFHC has to be extended (or other experimental models such as Ccl4 challenge should be taken into account).

Of note, it was also demonstrated that global ATGL KO mice are protected from acute ER stress development due to oleic acid enrichment in the liver [26]. Increased hepatic oleic acid concentration in MCD challenged liver specific ATGL KO mice suggests that reduced ER stress development is linked to a similar mechanism.

In addition to oleic acid, also α- and γ-linolenic acid are among the most abundant FAs found in livers of MCD fed ATGL LKO mice (Figure 5C). These three FA species are capable of activating PPARδ [39]. Accordingly, PPARδ DNA binding activity was also increased in this group of animals. Anti-inflammatory effects of PPARδ have been demonstrated in several preclinical NAFLD studies [40-42]. While PPARα activation depends on FAs derived from intracellular TG hydrolysis, PPARδ activation does not appear to be dependent on intracellular TG catabolism [16]. Therefore, augmented PPARδ activation in ATGL LKO mice may compensate for impaired PPARα signalling, thereby attenuating hepatic inflammation and subsequent progression from NAFLD to NASH. This observation is in line with the finding that PPARδ directly compensates for the absence of PPARα in regulating FA homeostasis in human and murine skeletal muscle cells [22].

Impaired PPARα signaling (seen in ATGL global [28] as well as in the ATGL LKO mice) was also found to be present in NASH patients where its expression correlates negatively with progression of the disease [43]. Longitudinal analysis showed that increase in expression of PPARα and its target genes was associated with histological improvement, underlining the use of PPARα agonists in the treatment of NASH [43]. Also PPARδ expression in NAFLD patients was investigated in several studies [43-45]. Interestingly, the findings are somewhat controversial. While in a small study it was shown that PPARδ expression was increased in NASH patients [44], in a larger cohort of NAFLD patients

PPARδ expression remained unchanged [43]. In line, we did not see changes in PPARδ protein expression (data not shown) in a cohort consisted of patients aged ≥18 years with biopsy-proven NASH, grouped into steatosis (F0), NASH early stage (F1-2) and NASH advanced stage (F3-4) [25]. However, if the patients are grouped based on the stage of fibrosis (NASH F1, NASH F2 and NASH F3) PPARδ protein expression tended to be reduced (Supporting Figure 11), arguing for a potential role of PPARδ as pharmacological target to counteract NAFLD progression. Thus, a clinical study investigating the effect of the PPARδ agonist seladelpar in NASH patients (F1-F3) showed an improvement of liver enzymes after 52 weeks of treatment [46].

Also, pharmacological inhibition of ATGL in adipose tissue with the specific inhibitor Atglistatin was proven to be beneficial in counteracting high-fat diet induced fatty liver development [47]. Inhibition of adipose tissue lipolysis may thus be favourable in strongly obese patients via reduction of FA flux to skeletal muscle and liver, thereby preventing ectopic lipid accumulation and insulin resistance. Here we show that loss of ATGL function also has beneficial effects in a lean mouse model of steatohepatitis. MCD diet promotes intrahepatic lipid accumulation mainly through increased hepatic fatty acid uptake and decreased VLDL secretion and, apparently, lipotoxic effects can be reduced by inhibition of lipolysis in hepatocytes promoting FA storage and neutralisation in the form of inert TG.

Interestingly, despite its close homology with adiponutrin/PNPLA3 (which has been found to be associated with development and progression of NAFLD/NASH and many other liver diseases [48]), for ATGL/PNPLA2 polymorphisms no convincing evidence for a role in fatty liver development was found. However, it has been shown that PNPLA3 effectively competes with ATGL for α/β hydrolase domain-containing 5 (ABHD5/CGI-58), an essential co-activator of ATGL and that PNPLA3 I148M is more effective in this regard [49], thus weakening lipolytic function of ATGL, favoring lipid accumulation. In contrast to PNPLA3 variants, PNPLA2 variants were associated with anthropometric and metabolic parameters such as fat mass and subcutaneous adipose tissue [50].

In vitro experiments revealed that loss of ATGL in hepatocytes have a direct anti-inflammatory effect, reducing secretion of pro-inflammatory cytokines and thereby

ameliorating immune cell recruitment/activation corroborating findings in liver ATGL deficiency. In line, also ATGL deficient macrophages have been identified to have reduced inflammatory activity [51] and increased lipolysis which induces macrophage migration [52].

In conclusion, our study provides profound evidence that inhibition of ATGL exclusively in the liver decelerates the progression of NAFLD from simple steatosis to more severe disease stages such as steatohepatitis. Therefore, ATGL inhibitors may be considered as useful strategy to combat NASH development.

References

1. Yang, L. and G.A. Colditz, *Prevalence of Overweight and Obesity in the United States, 2007-2012.* JAMA Intern Med, 2015. **175**(8): p. 1412-3.
2. Ogden, C.L., et al., *Prevalence of overweight and obesity in the United States, 1999-2004.* JAMA, 2006. **295**(13): p. 1549-55.
3. Williams, C.D., et al., *Prevalence of nonalcoholic fatty liver disease and nonalcoholic steatohepatitis among a largely middle-aged population utilizing ultrasound and liver biopsy: a prospective study.* Gastroenterology, 2011. **140**(1): p. 124-31.
4. Schreuder, T.C., et al., *Nonalcoholic fatty liver disease: an overview of current insights in pathogenesis, diagnosis and treatment.* World J Gastroenterol, 2008. **14**(16): p. 2474-86.
5. Cohen, J.C., J.D. Horton, and H.H. Hobbs, *Human fatty liver disease: old questions and new insights.* Science, 2011. **332**(6037): p. 1519-23.
6. Angulo, P., *Nonalcoholic fatty liver disease.* N Engl J Med, 2002. **346**(16): p. 1221-31.
7. Tacke, F., T. Luedde, and C. Trautwein, *Inflammatory pathways in liver homeostasis and liver injury.* Clin Rev Allergy Immunol, 2009. **36**(1): p. 4-12.
8. Marra, F. and G. Svegliati-Baroni, *Lipotoxicity and the gut-liver axis in NASH pathogenesis.* J Hepatol, 2018. **68**(2): p. 280-295.
9. Neuschwander-Tetri, B.A., *Hepatic lipotoxicity and the pathogenesis of nonalcoholic steatohepatitis: the central role of nontriglyceride fatty acid metabolites.* Hepatology, 2010. **52**(2): p. 774-88.
10. Zechner, R., et al., *FAT SIGNALS--lipases and lipolysis in lipid metabolism and signaling.* Cell Metab, 2012. **15**(3): p. 279-91.
11. Varga, T., Z. Czimmerer, and L. Nagy, *PPARs are a unique set of fatty acid regulated transcription factors controlling both lipid metabolism and inflammation.* Biochim Biophys Acta, 2011. **1812**(8): p. 1007-22.
12. Ong, K.T., et al., *Adipose triglyceride lipase is a major hepatic lipase that regulates triacylglycerol turnover and fatty acid signaling and partitioning.* Hepatology, 2011. **53**(1): p. 116-26.
13. Haemmerle, G., et al., *ATGL-mediated fat catabolism regulates cardiac mitochondrial function via PPAR-alpha and PGC-1.* Nat Med, 2011. **17**(9): p. 1076-85.
14. Wu, J.W., et al., *Deficiency of liver adipose triglyceride lipase in mice causes progressive hepatic steatosis.* Hepatology, 2011. **54**(1): p. 122-32.

15. Sanderson, L.M., et al., *Transcriptional profiling reveals divergent roles of PPARalpha and PPARbeta/delta in regulation of gene expression in mouse liver.* Physiol Genomics, 2010. **41**(1): p. 42-52.
16. Sanderson, L.M., et al., *Peroxisome proliferator-activated receptor beta/delta (PPARbeta/delta) but not PPARalpha serves as a plasma free fatty acid sensor in liver.* Mol Cell Biol, 2009. **29**(23): p. 6257-67.
17. Tang, T., et al., *Desnutrin/ATGL activates PPARdelta to promote mitochondrial function for insulin secretion in islet beta cells.* Cell Metab, 2013. **18**(6): p. 883-95.
18. Dubois, V., et al., *Distinct but complementary contributions of PPAR isotypes to energy homeostasis.* J Clin Invest, 2017. **127**(4): p. 1202-1214.
19. Ip, E., et al., *Central role of PPARalpha-dependent hepatic lipid turnover in dietary steatohepatitis in mice.* Hepatology, 2003. **38**(1): p. 123-32.
20. Ip, E., et al., *Administration of the potent PPARalpha agonist, Wy-14,643, reverses nutritional fibrosis and steatohepatitis in mice.* Hepatology, 2004. **39**(5): p. 1286-96.
21. Staels, B., et al., *Hepatoprotective effects of the dual peroxisome proliferator-activated receptor alpha/delta agonist, GFT505, in rodent models of nonalcoholic fatty liver disease/nonalcoholic steatohepatitis.* Hepatology, 2013. **58**(6): p. 1941-52.
22. Muoio, D.M., et al., *Fatty acid homeostasis and induction of lipid regulatory genes in skeletal muscles of peroxisome proliferator-activated receptor (PPAR) alpha knock-out mice. Evidence for compensatory regulation by PPAR delta.* J Biol Chem, 2002. **277**(29): p. 26089-97.
23. Jha, P., et al., *Role of adipose tissue in methionine-choline-deficient model of non-alcoholic steatohepatitis (NASH).* Biochim Biophys Acta, 2014. **1842**(7): p. 959-70.
24. Sitnick, M.T., et al., *Skeletal muscle triacylglycerol hydrolysis does not influence metabolic complications of obesity.* Diabetes, 2013. **62**(10): p. 3350-61.
25. Jha, P., et al., *Genetic Regulation of Plasma Lipid Species and Their Association with Metabolic Phenotypes.* Cell Syst, 2018. **6**(6): p. 709-721 e6.
26. Fuchs, C.D., et al., *Absence of adipose triglyceride lipase protects from hepatic endoplasmic reticulum stress in mice.* Hepatology, 2012. **56**(1): p. 270-80.
27. Liang, W., et al., *Establishment of a general NAFLD scoring system for rodent models and comparison to human liver pathology.* PLoS One, 2014. **9**(12): p. e115922.
28. Jha, P., et al., *Role of adipose triglyceride lipase (PNPLA2) in protection from hepatic inflammation in mouse models of steatohepatitis and endotoxemia.* Hepatology, 2014. **59**(3): p. 858-69.

29. Verkade, H.J., et al., *Fat absorption in neonates: comparison of long-chain-fatty-acid and triglyceride compositions of formula, feces, and blood.* Am J Clin Nutr, 1991. **53**(3): p. 643-51.
30. Liss, K.H. and B.N. Finck, *PPARs and nonalcoholic fatty liver disease.* Biochimie, 2017. **136**: p. 65-74.
31. Fyffe, S.A., et al., *Recombinant human PPAR-beta/delta ligand-binding domain is locked in an activated conformation by endogenous fatty acids.* J Mol Biol, 2006. **356**(4): p. 1005-13.
32. Fyffe, S.A., et al., *Reevaluation of the PPAR-beta/delta ligand binding domain model reveals why it exhibits the activated form.* Mol Cell, 2006. **21**(1): p. 1-2.
33. Souza, C.O., et al., *Palmitoleic acid (n-7) attenuates the immunometabolic disturbances caused by a high-fat diet independently of PPARalpha.* Mediators Inflamm, 2014. **2014**: p. 582197.
34. Rubio, C., et al., *Impact of global PTP1B deficiency on the gut barrier permeability during NASH in mice.* Mol Metab, 2020. **35**: p. 100954.
35. Rinella, M.E., et al., *Mechanisms of hepatic steatosis in mice fed a lipogenic methionine choline-deficient diet.* J Lipid Res, 2008. **49**(5): p. 1068-76.
36. Henao-Mejia, J., et al., *Inflammasome-mediated dysbiosis regulates progression of NAFLD and obesity.* Nature, 2012. **482**(7384): p. 179-85.
37. Hebbard, L. and J. George, *Animal models of nonalcoholic fatty liver disease.* Nat Rev Gastroenterol Hepatol, 2011. **8**(1): p. 35-44.
38. Donnelly, K.L., et al., *Sources of fatty acids stored in liver and secreted via lipoproteins in patients with nonalcoholic fatty liver disease.* J Clin Invest, 2005. **115**(5): p. 1343-51.
39. Ravnskjaer, K., et al., *PPARdelta is a fatty acid sensor that enhances mitochondrial oxidation in insulin-secreting cells and protects against fatty acid-induced dysfunction.* J Lipid Res, 2010. **51**(6): p. 1370-9.
40. Lee, M.Y., et al., *Peroxisome proliferator-activated receptor delta agonist attenuates hepatic steatosis by anti-inflammatory mechanism.* Exp Mol Med, 2012. **44**(10): p. 578-85.
41. Haczeyni, F., et al., *The selective peroxisome proliferator-activated receptor-delta agonist seladelpar reverses nonalcoholic steatohepatitis pathology by abrogating lipotoxicity in diabetic obese mice.* Hepatol Commun, 2017. **1**(7): p. 663-674.
42. Nagasawa, T., et al., *Effects of bezafibrate, PPAR pan-agonist, and GW501516, PPARdelta agonist, on development of steatohepatitis in mice fed a methionine- and choline-deficient diet.* Eur J Pharmacol, 2006. **536**(1-2): p. 182-91.
43. Francque, S., et al., *PPARalpha gene expression correlates with severity and histological treatment response in patients with non-alcoholic steatohepatitis.* J Hepatol, 2015. **63**(1): p. 164-73.

44. Pettinelli, P. and L.A. Videla, *Up-regulation of PPAR-gamma mRNA expression in the liver of obese patients: an additional reinforcing lipogenic mechanism to SREBP-1c induction.* J Clin Endocrinol Metab, 2011. **96**(5): p. 1424-30.
45. Lima-Cabello, E., et al., *Enhanced expression of pro-inflammatory mediators and liver X-receptor-regulated lipogenic genes in non-alcoholic fatty liver disease and hepatitis C.* Clin Sci (Lond), 2011. **120**(6): p. 239-50.
46. Harrison, S.A., et al., *A 52-Week Multi-Center Double-Blind Randomized Phase 2 Study Of Seladelpar, A Potent And Selective Peroxisome Proliferator-Activated Receptor Delta (PPAR-Delta) Agonist, In Patients With Nonalcoholic Steatohepatitis (NASH).* Hepatology, 2020. **72**(1): p. 1043A-1044A.
47. Schweiger, M., et al., *Pharmacological inhibition of adipose triglyceride lipase corrects high-fat diet-induced insulin resistance and hepatosteatosis in mice.* Nat Commun, 2017. **8**: p. 14859.
48. Romeo, S., et al., *Genetic variation in PNPLA3 confers susceptibility to nonalcoholic fatty liver disease.* Nat Genet, 2008. **40**(12): p. 1461-5.
49. Yang, A., et al., *Dynamic interactions of ABHD5 with PNPLA3 regulate triacylglycerol metabolism in brown adipocytes.* Nat Metab, 2019. **1**(5): p. 560-569.
50. Zegers, D., et al., *Association study of PNPLA2 gene with histological parameters of NAFLD in an obese population.* Clin Res Hepatol Gastroenterol, 2016. **40**(3): p. 333-339.
51. Aflaki, E., et al., *Impaired Rho GTPase activation abrogates cell polarization and migration in macrophages with defective lipolysis.* Cell Mol Life Sci, 2011. **68**(23): p. 3933-47.
52. Radovic, B., E. Aflaki, and D. Kratky, *Adipose triglyceride lipase in immune response, inflammation, and atherosclerosis.* Biol Chem, 2012. **393**(9): p. 1005-11.

Figure Legends

Figure 1: MCD-feeding induced liver injury in WT and ATGL LKO mice. Wildtype (WT) and ATGL knockout (KO) mice received methionine choline deficient (MCD) diet for 5 weeks. (A) H&E staining of liver sections of control and MCD-fed WT and ATGL LKO mice. Hepatic steatosis was evident in ATGL LKO mice at baseline and even more pronounced after MCD challenge. (B) Biochemical quantification of intrahepatic triglyceride (TG). Intrahepatic TG levels were increased in ATGL LKO mice at baseline as well as in MCD treated WT and ATGL LKO mice. (C) Oil red O staining. Oil red O (ORO) staining and subsequent computational quantification displayed elevated intrahepatic lipid accumulation in ATGL LKO mice at baseline. MCD feeding increased lipid load in both genotypes. (D) Serum markers of liver injury. MCD diet-induced liver injury was reflected by increased levels of liver enzymes (AST; ALT) and alkaline phosphatase (AP) in WT and ATGL LKO mice. Serum total cholesterol and triglycerides (TG), as well as NEFAs were significantly reduced after MCD feeding. * indicates a significant difference from untreated WT controls (WT); # indicates a significant difference from ATGL LKO KO control mice; $p<0,05$.

Figure 2: MCD feeding-induced hepatic inflammation and ER stress is attenuated in ATGL LKO mice. (A) MAC-2 immunohistochemistry. Representative immunohistochemistry stainings for MAC-2^+ cells in liver specimens of control and MCD-fed WT and ATGL LKO mice (20x magnification) as well as computational quantification show increased inflammation in MCD-fed WT mice. (B) MPO immunofluorescence. Representative immunofluorescence stainings for MPO^+ cells in liver specimens of control and MCD-fed WT and ATGL LKO mice (20x magnification) as well as computational quantification show increased inflammation in MCD-fed WT mice. (C) Representative picture of ER stress sensor immune blots. Protein expression levels of PERK and IRE1α were elevated in WT MCD fed mice and stayed at baseline levels in ATGL LKO MCD fed mice. Data are normalised to total protein and represent means +/-

SD and are shown relatively to the expression levels of unchallenged WT animals. Data represent means +/- SD and are shown relatively to the expression levels of unchallenged WT animals. * indicates a significant difference from untreated WT controls; $ indicates a significant difference from MCD-fed WT mice; # indicates a significant difference from ATGL LKO controls; p<0,05.

Figure 3: MCD feeding increases PPARδ activity in ATGL LKO mice. (A) Semiquantitative PPARδ DNA binding activity assay. MCD feeding induced PPARδ signalling in ATGL LKO (but not in WT) mice. (B) mRNA expression levels of PPARδ downstream target *Pdk4*. mRNA expression of *Pdk4* was increased due to MCD feeding in both genotypes but the increase was more pronounced in ATGL LKO mice. Data represent means +/- SD and are shown relatively to the expression levels of unchallenged WT animals. (C) Representative picture of PPARδ downstream target PDK4 immune blot. Protein expression levels of PDK4 were elevated in WT MCD fed mice and stayed at baseline levels in ATGL LKO MCD fed mice. Data are normalised to total protein and represent means +/- SD and are shown relatively to the expression levels of unchallenged WT animals. (D) Intrahepatic free fatty acid profile. α- and γ-Linolenic acid (known to be PPARδ ligands) were most prominent in ATGL LKO MCD fed animals. * indicates a significant difference from untreated WT controls; $ indicates a significant difference from MCD-fed WT mice; # indicates a significant difference from ATGL LKO controls; p<0,05.

Figure 4: HFHC-feeding induced liver injury in WT and ATGL LKO mice. Wildtype (WT) and ATGL knockout (KO) mice received high fat high carbohydrate (HFHC) diet for 17 weeks. (A) H&E staining of liver sections of control and HFHC-fed WT and ATGL LKO mice. Hepatic steatosis was evident in ATGL LKO mice at baseline and even more pronounced after HFHC challenge (20x magnification). (B) Biochemical quantification of intrahepatic triglycerides (TG). Intrahepatic TG levels were increased in ATGL LKO mice at baseline as well as in HFHC treated WT and ATGL LKO mice. (C) Oil red O staining. Oil red O (ORO) staining and subsequent computational quantification displayed elevated

intrahepatic lipid accumulation in ATGL LKO mice at baseline. HFHC feeding increased lipid load in both genotypes with a more pronounced rise in ATGL LKO mice. (D) Serum markers of liver injury. 21 week old ATGL LKO mice showed increased levels of liver enzymes (AST, ALT) already at baseline. While HFHC feeding led to a further increase of transaminases in WT mice, in ATGL LKO mice the levels remained unaffected. Alkaline phosphatase (AP) and triglyceride levels remained constant in WT and ATGL LKO mice. Serum total cholesterol and non-esterified fatty acids (NEFAs) were significantly increased after HFHC feeding. * indicates a significant difference from untreated WT controls (WT); # indicates a significant difference from ATGL LKO control mice; p<0,05.

Figure 5: HFHC feeding-induced hepatic inflammation and ER stress is attenuated in ATGL LKO mice. (A) MAC-2 immunohistochemistry. Representative immunohistochemistry staining for MAC-2$^+$ cells in liver specimens of control and HFHC-fed WT and ATGL LKO mice (20x magnification) as well as computational quantification show increased inflammation in HFHC-fed WT and ATGL LKO mice. ATGL LKO HFHC fed mice show significant less MAC-2$^+$ cells compared to WT mice upon HFHC treatment. (B) MPO immunofluorescence. Representative immunofluorescence staining for MPO$^+$ cells in liver specimens of control and HFHC-fed WT and ATGL LKO mice (20x magnification) as well as computational quantification show increased inflammation in HFHC-fed WT and ATGL LKO mice. ATGL LKO HFHC fed mice show significant less MPO$^+$ cells compared to WT mice upon HFHC treatment. (C) Representative picture of ER stress sensor immune blots. Protein expression levels of PERK and IRE1α were elevated in both, WT and ATGL LKO HFHC fed mice. Data are normalised to total protein and represent means +/- SD and are shown relatively to the expression levels of unchallenged WT animals. * indicates a significant difference from untreated WT controls; $ indicates a significant difference from MCD-fed WT mice; # indicates a significant difference from ATGL LKO controls; p<0,05.

Figure 6: HFHC feeding increases PPARδ activity in ATGL LKO mice. (A) Semiquantitative PPARδ DNA binding activity assay. HFHC feeding induced PPARδ

signalling in ATGL LKO (but not in WT) mice. (B) mRNA expression levels of PPARδ downstream target *Pdk4.* mRNA expression of *Pdk4* was increased due to HFHC feeding in in ATGL LKO mice. Data represent means +/- SD and are shown relatively to the expression levels of unchallenged WT animals. (C) Representative picture of PPARδ downstream target PDK4 immune blot. Protein expression levels of PDK4 were elevated in WT and ATGL LKO HFHC fed mice. Data are normalised to total protein and represent means +/- SD and are shown relatively to the expression levels of unchallenged WT animals. (D) Intrahepatic free fatty acid profile. α- and γ-Linolenic acid (known to be PPARδ ligands) concentration remained unchanged among the different groups while oleic acid concentration was increased in ATGL LKO mice at baseline, further increased by HFHC feeding in both, WT and ATGL LKO animals. * indicates a significant difference from untreated WT controls; $ indicates a significant difference from MCD-fed WT mice; # indicates a significant difference from ATGL LKO controls; p<0,05.

Figure 7: Knock down of ATGL protects from LPS induced inflammation and prevents from LPS induced cytokine secretion *in vitro.* (A) 6h after LPS challenge gene expression of inflammatory markers *Mcp1, Cxcl2* and *Tnfα* were significantly increased in HepG2 WT cells and did not change in HepG2 ATGL KD cells. Data represent means +/- SD and are shown relatively to the expression levels of untreated HepG2 WT cells. * indicates a significant difference from untreated HepG2 WT cells; $ indicates a significant difference from LPS treated HepG2 WT cells; # indicates a significant difference from untreated HepG2 ATGL KD cells; p<0,05. (B) Proteome profiling revealed that HepG2 ATGL KD cells secrete less cytokines/chemokines upon LPS stimulation. Cells were treated with LPS for 6h. Thereafter LPS containing medium was exchanged with empty medium. After 24h the medium was used for proteome profiling. HepG2 LPS treated cells secreted more Osteopontin, IL8, MiC1 and VEGF than HepG2 ATGL KD LPS treated cells. (C) Human macrophage cell line THP1 was cultered in medium taken from HepG2 WT cells and HepG2 ATGL KD cells treated with LPS for 6h. mRNA expression levels of *IL1b, IL6* and *Mcp1* were increased in THP1 cells treated with medium from HepG2 WT LPS cells but not in THP1 cells treated with medium from HepG2 ATGL KD LPS cells. Data represent means +/- SD and are shown relatively to the

expression levels of THP1 cells cultured medium form HepG2 WT cells. * indicates a significant difference from THP1 cells cultured in medium form HepG2 WT cells; # indicates a significant difference from THP1 cells cultured medium form HepG2 ATGL KD cells; $ indicates a significant difference from THP1 cells treated with LPS and cultured in medium from HepG2 WT cells; p<0,05.

Figure 8: Activation of PPARδ reduces LPS induced inflammation *in vitro.* (A and B) The human hepatoma cell line HepG2 were pre-treated with the PPARδ agonist GW0742 before 6h LPS exposure. (A) Representative picture of PPARδ downstream target PDK4 immune blot. Protein levels of the PPARδ downstream target PDK4 were significantly increased in cells treated with GW0742. (B) Representative picture of NF*k*B subunits p50 and p65 immune blots. 6h after LPS challenge protein expression of the NF*k*B subunits p50 and p65 were significantly decreased in LPS challenged cells pre-treated with GW0742. (C) Gene expression of NF*k*B downstream targets. 6h after LPS challenge gene expression of inflammatory markers *Mcp1, Cxcl2* and *Tnfα* were significantly decreased in LPS challenged cells pre-treated with GW0742. Data represent means +/- SD and are shown relatively to the expression levels of unchallenged HepG2 cells. * indicates a significant difference from untreated control cells (Ctrl); $ indicates a significant difference from LPS treated HepG2 cells; p<0,05.

Supporting Figure 1: Disturbed PPARα signalling in MCD fed ATGL LKO mice. (A) Semiquantitative PPARα DNA binding activity assay in chow and MCD fed mice. MCD feeding induced PPARα signalling in both, WT and ATGL LKO mice. PPARα DNA binding activity is significantly reduced in ATGL LKO MCD fed mice compared to WT MCD fed mice. (B) mRNA expression levels of PPARα downstream targets. mRNA levels of *Cyp4a14* and *Fgf21* were increased due to MCD feeding in both genotypes but the increase was less pronounced in ATGL LKO mice. Data represent means +/- SD and are shown relatively to the expression levels of unchallenged WT animals. * indicates a significant difference from untreated WT controls; $ indicates a significant difference from MCD-fed WT mice; # indicates a significant difference from ATGL LKO control mice; p<0,05.

Supporting Figure 2: MCD feeding-induced hepatic inflammation and ER stress are attenuated in ATGL LKO mice. (A) Gene expression profile of inflammatory markers. *IL1β, F4/80* and *TNFα* mRNA expression levels were increased due to MCD feeding in WT and ATGL LKO mice, but to a lesser extend in ATGL LKO mice. (B) Gene expression profile of ER stress markers. *Erdj4* and *Grp78* mRNA expression levels were increased due to MCD feeding in WT and ATGL LKO mice, but to a lesser extend in ATGL LKO mice. (C) Gene expression of apoptosis markers. mRNA levels of *Chop* and *Bad* are increased due to MCD feeding independent of the genotype. Data represent means +/- SD and are shown relatively to the expression levels of unchallenged WT animals. (D) Representative picture of cleaved caspase 3 immune blot. Protein expression levels of cleaved caspase 3 were elevated in WT MCD fed mice. Data are normalised to total protein and represent means +/- SD and are shown relatively to the expression levels of unchallenged WT animals. * indicates a significant difference from untreated WT controls; $ indicates a significant difference from MCD-fed WT mice; # indicates a significant difference from ATGL LKO control mice; p<0,05

Supporting Figure 3: Hepatic fibrosis is moderately increased due to MCD feeding. (A) Sirius red staining. Representative pictures of Sirius red staining do not show increased collagen deposition due to MCD feeding in WT and ATGL LKO mice. (B) Representative pictures of Collagen 1 immunohistochemistry did not show collagen deposition due to HFHC feeding in WT and ATGL LKO mice. (C) Gene expression profile of fibrotic markers. *Col1a1, Col1a2* and *Tgfβ* were assessed by qPCR. Expression of these genes was markedly increased in both, MCD-fed WT and ATGL LKO mice. Data represent means +/- SD and are shown relatively to the expression levels of unchallenged WT animals. * indicates a significant difference from untreated WT control animals; # indicates a significant difference from ATGL LKO control animals; p<0,05.

Supporting Figure 4: Intrahepatic fatty acid profile of anti-inflammatory fatty acids in the MCD and the HFHC setting. (A) Palmitoleic and Vaccenic acid**,** two anti-

inflammatory fatty acids (not related to PPAR signalling) are reduced in WT mice upon MCD feeding while in ATGL LKO MCD fed mice their concentration stayed at normal levels. (B) Palmitoleic and Vaccenic acid, two anti-inflammatory fatty acids (not related to PPAR signalling) are increased in ATGL LKO mice at baseline. While HFHC feeding led to an increase of the intrahepatic concentration of these FAs in WT mice, in ATGL LKO mice the levels remained unaffected. * indicates a significant difference from untreated WT control animals; $ indicates a significant difference from MCD-fed WT animals; p<0,05.

Supporting Figure 5: Disturbed PPARα signalling in HFHC fed ATGL LKO mice. (A) Semiquantitative PPARα DNA binding activity assay in chow and HFHC fed mice. HFHC feeding induced PPARα signalling in both, WT and ATGL LKO mice. PPARα DNA binding activity is significantly reduced in ATGL LKO MCD fed mice compared to WT HFHC fed mice. (B) mRNA expression levels of PPARα downstream targets. mRNA levels of *Cyp4a14* and *Fgf21* were increased due to HFHC feeding in both genotypes but the increase was less pronounced in ATGL LKO mice. Data represent means +/- SD and are shown relatively to the expression levels of unchallenged WT animals. * indicates a significant difference from untreated WT control animals; $ indicates a significant difference from MCD-fed WT mice; # indicates a significant difference from ATGL LKO control animals; p<0,05.

Supporting Figure 6: MCD feeding-induced hepatic inflammation and ER stress are attenuated in ATGL LKO mice. (A) Gene expression profile of inflammatory markers. *IL1β, F4/80* and *TNFα* mRNA expression levels were increased due to HFHC feeding in WT and ATGL LKO mice, but to a lesser extend in ATGL LKO mice (B) Gene expression profile of ER stress markers. *Erdj4* and *Grp78* mRNA expression levels were increased due to HFHC feeding in WT and ATGL LKO mice, but to a lesser extend in ATGL LKO mice. (C) Gene expression of apoptosis markers. mRNA levels of *Chop* and *Bad* are increased due to HFHC feeding. Data represent means +/- SD and are shown relatively to the expression levels of unchallenged WT animals. (D) Representative picture of cleaved caspase 3 immune blot. Protein expression levels of cleaved caspase 3

remained unchanged after HFHC fed mice. Data are normalised to total protein and represent means +/- SD and are shown relatively to the expression levels of unchallenged WT animals. * indicates a significant difference from untreated WT control animals; $ indicates a significant difference from MCD-fed WT animals; # indicates a significant difference from ATGL LKO control mice; p<0,05

Supporting Figure 7: Hepatic fibrosis is unaffected upon HFHC feeding. (A) Sirius red staining. Representative pictures of Sirius red staining do not show increased collagen deposition due to HFHC feeding in WT and ATGL LKO mice. (B) Representative pictures of Collagen 1 immunohistochemistry did not show collagen deposition due to HFHC feeding in WT and ATGL LKO mice. (C) Gene expression profile of fibrotic markers. *Col1a1, Col1a2* and *Tgfβ* were assessed by qPCR. Expression of these genes tended to be increased in HFHC-fed WT mice. Data represent means +/- SD and are shown relatively to the expression levels of unchallenged WT animals.

Figure 8: Knock down of ATGL in HepG2 and Hepa1c1c7 cells. The human hepatoma cell line HepG2 and the murine hepatocyte cell line Hepa1c1c7 were used to knock down (KD) ATGL with shRNA. (A) mRNA expression as well as (B) protein expression of ATGL are significantly reduced in HepG2 ATGL KD cells. (C) mRNA expression as well as (D) protein expression of ATGL are significantly reduced in Hepa1c1c7 ATGL KD cells. Data are normalised to total protein and represent means +/- SD and are shown relatively to the expression levels of unchallenged WT cells. * indicates a significant difference from untreated WT cells; p<0,05

Figure 9: Knock down of ATGL protects from LPS induced inflammation and prevents from LPS induced cytokine secretion *in vitro.* (A) 6h after LPS challenge gene expression of inflammatory markers *Mcp1, Cxcl2* and *Tnfα* were significantly increased in WT cells and did not change in Hepa1c1c7 ATGL KD cells. Data represent means +/- SD and are shown relatively to the expression levels of unchallenged

Hepa1c1c7 WT cells. * indicates a significant difference from untreated Hepa1c1c7 WT cells; $ indicates a significant difference from LPS treated Hepa1c1c7 WT cells; p<0,05. (B) Proteome profiling revealed that Hepa1c1c7 ATGL KD cells do not secrete cytokines/chemokines upon LPS stimulation. Cells were treated with LPS for 6h. Thereafter LPS containing medium was exchanged with empty medium. After 24h the medium was used for proteome profiling. While Hepa1c1c7 LPS treated cells secreted CXCL-1, M-CSF, MCP1/CCL-2 and Rantes/CCL-5, Hepa1c1c7 ATGL KD LPS treated cells did not. (C) Murine macrophage cell line RAW264.7 was cultered in medium taken from Hepa1c1c7 WT cells and Hepa1c1c7 ATGL KD cells treated with/without LPS for 6h. mRNA expression levels of *IL1b, IL6* and *Mcp1* were increased in RAW246.7 cells treated with medium from Hepa1c1c7 WT LPS cells but not in RAW246.7 cells treated with medium from Hepa1c1c7 ATGL KD LPS cells. Data represent means +/- SD and are shown relatively to the expression levels of RAW264.7 cells cultured in medium taken from untreated Hepa1c1c7 WT cells. * indicates a significant difference from RAW264.7 cells cultured in Medium taken from LPS treated Hepa1c1c7 WT cells; $ indicates a significant difference from LPS treated control cellsp<0,05.

Supporting Figure 10: Knock down of ATGL protects from OP21 induced inflammation and prevents from LPS induced cytokine secretion *in vitro.* (A) 24h after OP21 challenge gene expression of inflammatory markers *Mcp1, Il1b, IL6* and *Cxcl2* were significantly increased in WT cells and did not change in HepG2 ATGL KD cells. Data represent means +/- SD and are shown relatively to the expression levels of unchallenged HepG2 WT cells. * indicates a significant difference from untreated HepG2 WT cells; $ indicates a significant difference from LPS treated HepG2 WT cells; p<0,05. (B) Proteome profiling revealed that HepG2 ATGL KD cells do not secrete cytokines/chemokines upon OP21 stimulation. Cells were treated with OP21 for 24h. Thereafter OP21 containing medium was exchanged with empty medium. After 24h cell the medium was used for proteome profiling. While HepG2 OP21 treated cells secreted Osteopontin and IL8, HepG2 ATGL KD OP21 treated cells did not. (C) Human macrophage cell line THP1 was cultured in medium taken from HepG2 WT cells and HepG2 ATGL KD cells treated with/without OP21 for 24h. mRNA expression levels of

IL1b, IL6 and *Mcp1* were increased in THP1 cells treated with medium from HepG2 WT OP21 treated cells but not in THP1 cells treated with medium from HepG2 ATGL KD OP21 treated cells. Data represent means +/- SD and are shown relatively to the expression levels of untreated THP1 cells. * indicates a significant difference from untreated THP1 cells; $ indicates a significant difference from THP1 cells cultured in medium from HepG2 WT OP21 treated cells; p<0,05.

Supporting Figure 11: PPARδ expression in human NASH samples. PPARδ expression was assessed immunohistochemically in human liver section of NAFLD patients. With progression of the disease, from NASH with fibrosis stage 1 to NASH with fibrosis stage 3 PPARδ expression decreases.

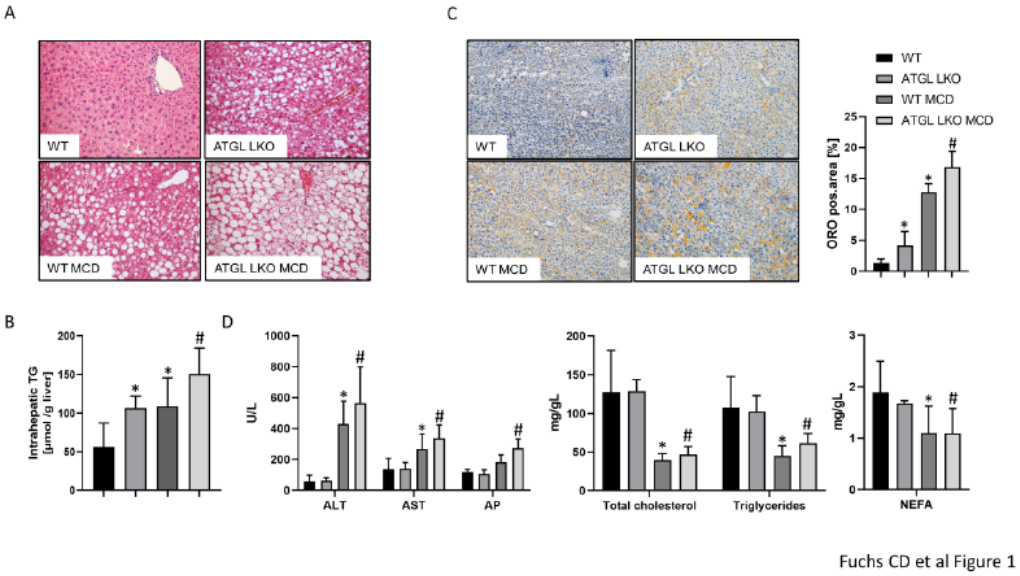

hep_32112_f1.tif

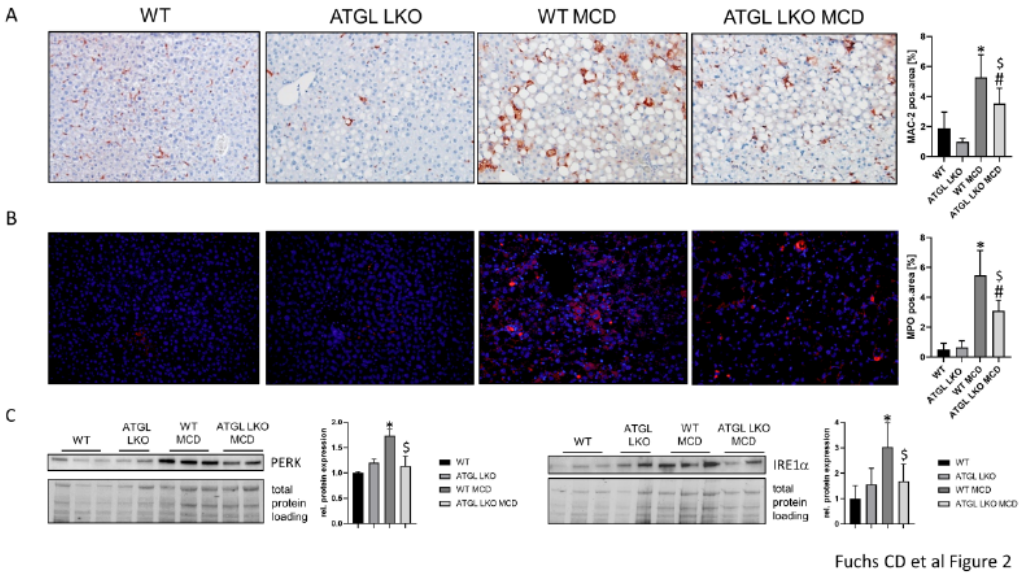

hep_32112_f2.tif

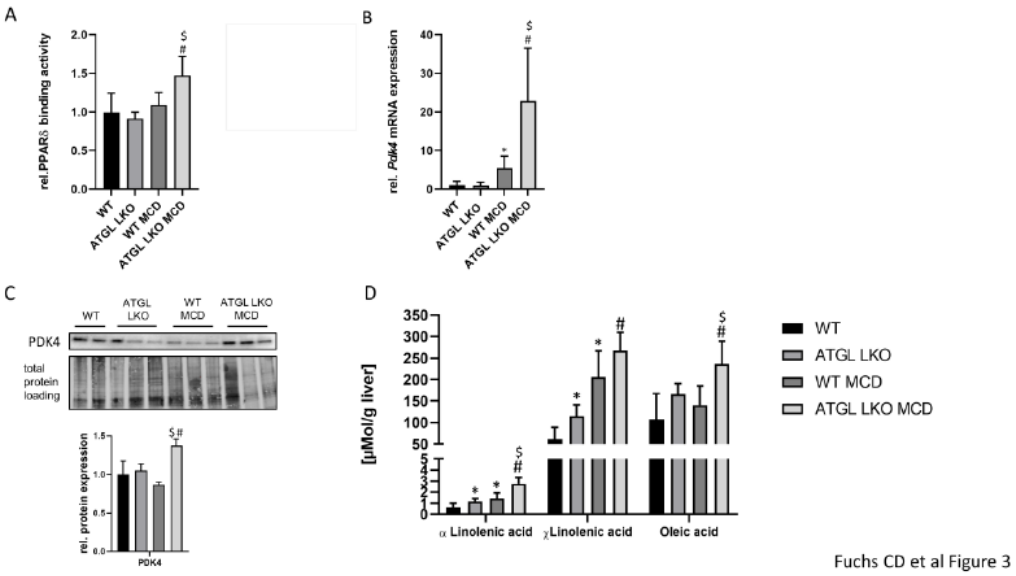

hep_32112_f3.tif

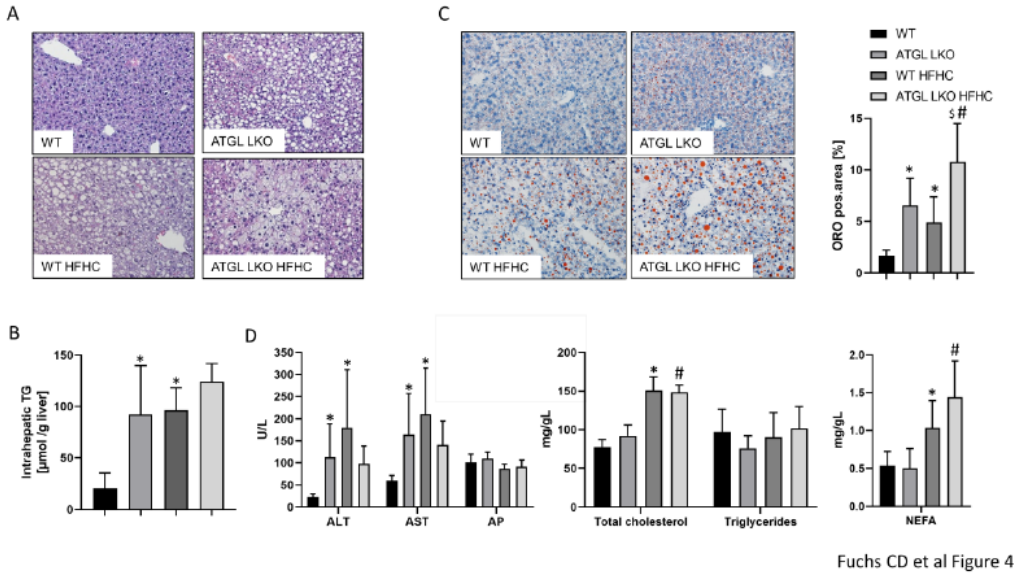

hep_32112_f4.tif

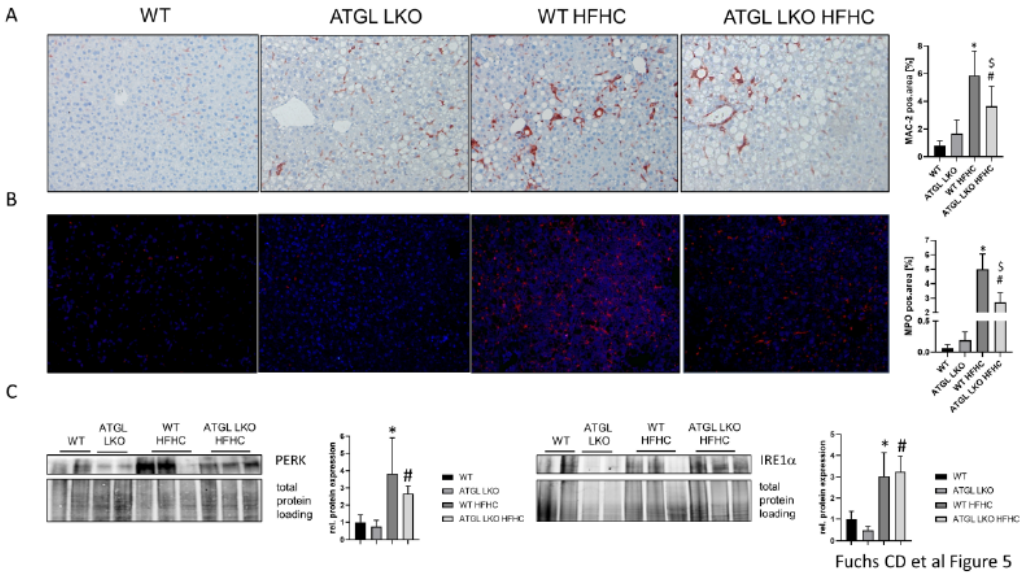

hep_32112_f5.tif

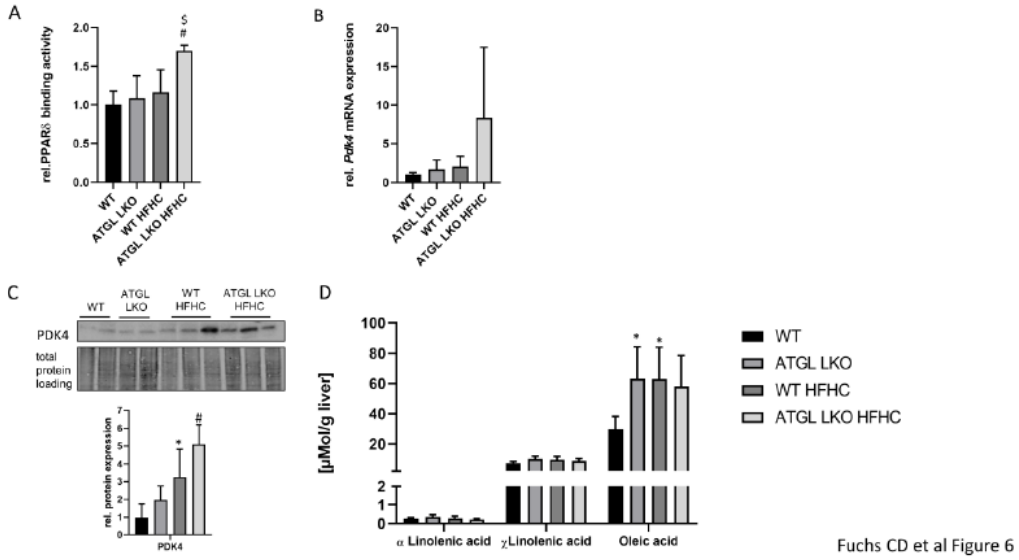

hep_32112_f6.tif

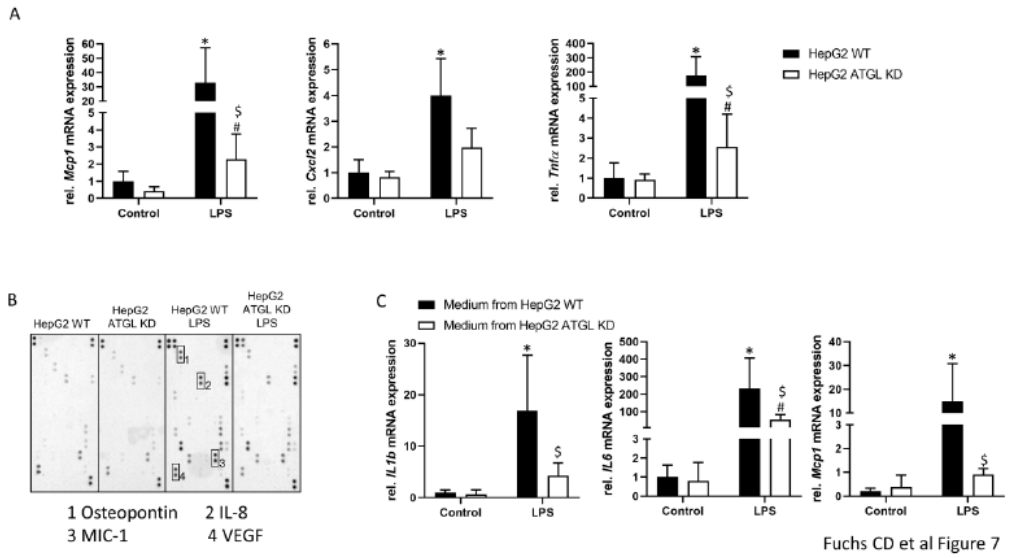

hep_32112_f7.tif

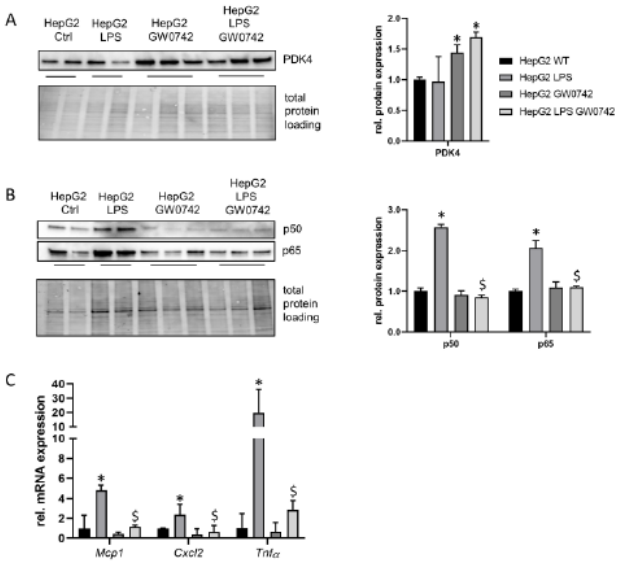

Fuchs CD et al Figure 8

hep_32112_f8.tif